ISSN 1063-7842, Technical Physics, 2017, Vol. 62, No. 2, pp. 223–229. © Pleiades Publishing, Ltd., 2017.
Original Russian Text © G.G. Bondarenko, M.R. Fisher, V.I. Kristya, 2017, published in Zhurnal Tekhnicheskoi Fiziki, 2017, Vol. 62, No. 2, pp. 197–203.

PLASMA

Influence of Temperature on the Ionization Coefficient and Ignition Voltage of the Townsend Discharge in an Argon–Mercury Vapor Mixture

G. G. Bondarenko[a], M. R. Fisher[b], and V. I. Kristya*[b]

[a] *National Research University Higher School of Economics, Myasnitskaya ul. 20, Moscow, 101000 Russia*

[b] *Bauman Moscow State Technical University (Kaluga branch), ul. Bazhenova 2, Kaluga, 248000 Russia*

**e-mail: kristya@bmstu-kaluga.ru*

Received June 7, 2016

Abstract—The kinetics of main types of charged and excited particles present in a low-current discharge in an argon–mercury vapor mixture used in gas-discharge illuminating lamps has been investigated in a wide interval of the reduced electric field strength and temperature. Mechanisms behind the production and loss of ions and metastable atoms have been discovered, and the temperature dependences of their contributions to maintaining their balance have been determined. It has been shown that, when the discharge is initiated in the lamp and the mercury content in the mixture is low, the ionization coefficient exceeds that in pure argon, which is almost exclusively due to the Penning reaction. The influence of this reaction grows with a reduction of the electric field strength in the interelectrode gap. The dependences of the discharge ignition voltage on the interelectrode gap (Paschen curves) for different temperatures of the mixture have been calculated, and the nonmonotonicity of the temperature dependence of the ignition voltage has been explained.

DOI: 10.1134/S1063784217020050

INTRODUCTION

Despite today's explosive development of LED technologies, gas-discharge lamps remain the main representatives of lighting devices [1–3]. As a working mixture, they usually use a mixture of argon with a density that corresponds to a pressure of 10^2–10^4 Pa at room temperature and mercury vapor with a density that depends on temperature. When the lamp is switched on, a voltage applied to the interelectrode gap causes a gas breakdown in it, and a low-current (Townsend) discharge is initiated, which subsequently changes to a glow discharge with a cathode fall of several hundred volts. The bombardment of the cathode by ions accelerated in the cathode sheath of the glow discharge results in electron emission from its surface, which maintains the discharge. In addition, the cathode's surface is heated and the emissive material is sputtered. When the cathode becomes hot, the thermionic emission from its surface begins and the discharge takes the arc form. The cathode fall of the arc discharge is much smaller than that of the glow discharge [4–6]. The most intense sputtering of the cathode, which leads to the loss of the emissive material and reduces its lifetime, takes place before the discharge transition to an arc, since the lifetime of the lamp operating in the continuous mode far exceeds its lifetime in the periodic on/off operating mode [7, 8].

The breakdown voltage, as well as the ignition voltage of the glow discharge (which greatly influences the bombarding ion energy), depends on the electron emission from the cathode and working gas ionization in the discharge volume. The former process is characterized by the effective coefficient of ion-electron emission, which equals the mean number of emitted electrons per ion incident on the cathode. The latter is characterized by the ionization coefficient, which is equal to the number of ionizations of working gas atoms per electron per unit length of the discharge. The feature of the argon–mercury vapor mixture is that mercury atoms are ionized not only in direct collisions with electrons but also in collisions with metastable excited argon atoms (Penning reaction) [9, 10]. As a result, the ionization coefficient and the discharge ignition voltage depend on temperature, because the mercury content in the mixture grows with increasing temperature. Thus, processes that take place under the current flow in the argon–mercury vapor mixture are of considerable interest. However, this issue has been given little attention so far. In [11, 12], the ionization coefficient was measured in a low-current discharge between planar electrodes for differ-

Ion–atom and atom–atom interactions included in the model and their rate constants

Reaction	Rate constant	Reference
$Ar^+ + 2Ar \rightarrow Ar_2^+ + Ar$	2.7×10^{-43} m^6 s^{-1}	[27]
$Hg^+ + 2Hg \rightarrow Hg_2^+ + Hg$	1.0×10^{-43} m^6 s^{-1}	[16]
$Ar^* + Ar^* \rightarrow Ar_2^+ + e$	5.7×10^{-16} m^3 s^{-1}	[27]
$Ar^* + Ar^* \rightarrow Ar^+ + Ar + e$	6.2×10^{-16} m^3 s^{-1}	[28]
$Hg^* + Hg^* \rightarrow Hg_2^+ + e$	$1.0 \times 10^{-20}\, v_a$ m^3 s^{-1}	[29]
$Hg^* + Hg^* \rightarrow Hg^+ + Hg + e$	$2.4 \times 10^{-19}\, v_a$ m^3 s^{-1}	[15]
$Ar^* + Hg \rightarrow Ar + Hg^+ + e$	9.0×10^{-16} m^3 s^{-1}	[30]
$Ar^+ + Hg \rightarrow Ar + Hg^+$	1.5×10^{-17} m^3 s^{-1}	[19]
$Ar^* + Ar \rightarrow 2Ar$	3.0×10^{-21} m^3 s^{-1}	[28]
$Hg^* + Hg \rightarrow 2Hg$	$8.0 \times 10^{-21}\, v_a$ m^3 s^{-1}	[31]
$Hg^* + Ar \rightarrow Hg^{**} + Ar$	$2.0 \times 10^{-24}\, v_a$ m^3 s^{-1}	[32]
$Ar^* + 2Ar \rightarrow Ar_2 + Ar$	1.1×10^{-43} m^6 s^{-1}	[28]
$Hg^* + 2Hg \rightarrow Hg_2 + Hg$	1.6×10^{-43} m^6 s^{-1}	[33]
$Ar^+ + e \rightarrow Ar^{**} + h\nu$	1.0×10^{-17} m^3 s^{-1}	[26]
$Hg^+ + e \rightarrow Hg^{**} + h\nu$	1.0×10^{-14} m^3 s^{-1}	[34]
$Ar_2^+ + e \rightarrow Ar^{**} + Ar$	$8.5 \times 10^{-13}(T/T_e)^{0.67}$ m^3 s^{-1}	[27]
$Hg_2^+ + e \rightarrow Hg^{**} + Hg$	$4.2 \times 10^{-13}(T/T_e)^{1.1}$ m^3 s^{-1}	[16]

Here, v_e is the average relative velocity of interacting atoms; T_e, electron temperature (K); T, temperature of the mixture (K).

ent relative mercury densities and electric field strengths in the interelectrode gap. In [13], the dependences of the ionization coefficient and contributions to it from different types of particle–particle interactions on the reduced electric field strength were calculated. The electron density was found from the condition of correspondence between calculation results and experimental data obtained in [11], and the densities of ions and excited atoms were determined from volume-averaged equations of their balance. The influence of different interactions in the argon–mercury vapor mixture was investigated only in the positive column of an arc discharge [14–18], for which low electric field strengths and electron mean energies are typical. In [19], breakdown in the lamp bulb was simulated and the corresponding processes at several fixed values of the relative mercury content were studied. In a number of works (see, e.g., [10, 12]), it was found that the temperature dependence of the discharge ignition voltage in this mixture is nonmonotonic: the voltage rises at near-room temperatures and decreases at higher values observed for some time after arc quenching in the lamp. However, detailed investigations of how different particle–particle interactions influence the discharge characteristics in an argon–mercury vapor mixture at the stage of discharge ignition at various temperatures have not been fulfilled to date.

In this work, we calculated the transport of electrons, ions, and metastable excited atoms in a low-current discharge initiated in an argon–mercury vapor mixture for a wide interval of the reduced electric field strength and temperature. The densities of charged and excited particles in the discharge gap were determined, and the contributions of different particle–particle interactions in maintaining their balance as functions of the relative mercury content in the mixture were estimated. Finally, the discharge ignition voltage was calculated at different temperatures of the working gas.

DISCHARGE MODEL

Let voltage U be applied to planar parallel electrodes with distance d between them. It is assumed that distance d is much smaller than the transverse size of the electrodes and voltage U is sufficient to initiate breakdown in the interelectrode gap, which is filled with argon having density n_{Ar} and saturated mercury vapor with density n_{Hg}. The z coordinate axis is directed normally to the electrodes, the cathode surface coincides with the plane $z = 0$, and the anode surface coincides with the plane $z = d$. Initially, current density j in the discharge is low and therefore the space charge does not distort the electric field distribution in

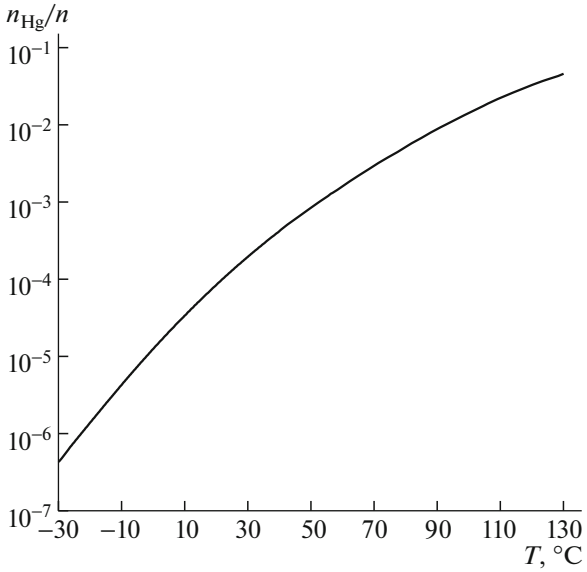

Fig. 1. Relative content of saturated mercury vapor in the argon–mercury mixture vs. temperature for $n_{Ar} = 6.57 \times 10^{23}$ m^{-3} [39].

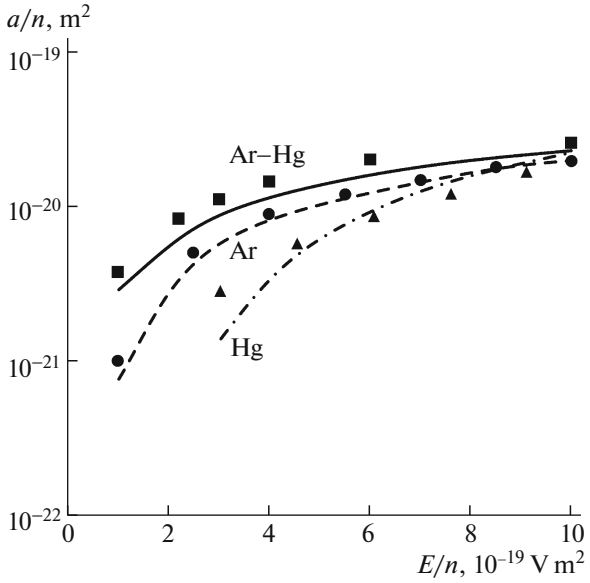

Fig. 2. Ionization coefficient vs. the reduced electric field strength in argon (dashed line), in mercury (dash-and-dot line), and in their mixture at $n_{Hg}/n = 6 \times 10^{-3}$ (solid line). Symbols ●, ▲, and ■ are experimental data points for the ionization coefficient of argon [41], mercury [42], and argon–mercury mixture [13], respectively.

the interelectrode gap. The field is parallel to the z axis everywhere in the gap and equals $E = U/d$, i.e., the discharge is low-current [5, 6].

Under the action of the electric field, electrons that are generated under the ionization of atoms are accelerated toward the anode, and ions move toward the cathode. In the course of motion, both types of particles collide with neutrals. In this work, the electron motion is simulated using the Monte Carlo method [20–22]. The elastic scattering of electrons by the atoms of mixture components, as well as the electron ionization and electron excitation of unexcited and metastable atoms, is taken into account with regard to the dependences of the cross sections of these processes on the electron velocity [23–25]. Having calculated the trajectories of primary and secondary electrons (i.e., emitted from the cathode and generated in the interelectrode gap under the ionization of mixture component atoms), we constructed their velocity distribution function $f_e(z_i, v, v_z)$ in each of s-intervals of length $\Delta z = d/s$, into which the interelectrode gap was divided. Here, $z_i = (i - 0.5)\Delta z$, ($i = 1, ..., s$) and v and v_z are the electron velocity and its longitudinal component, respectively.

The main types of ions in a low-current discharge initiated in an argon–mercury vapor mixture are atomic and molecular ions of both components: Ar^+, Ar_2^+, Hg^+, and Hg_2^+ [19, 26]. Of the excited atoms, argon metastables 4^3P_0 and 4^3P_2, as well as mercury metastables 6^3P_0 and 6^3P_2, have the highest densities. Since the energy levels of the two metastsables of either gas are close to each other, they can be considered as identical (they are designated Ar* and Hg*, respectively) [13, 19, 27]. As for atoms that are excited to resonance levels (Ar** and Hg**, respectively), they are rapidly deexcited, and therefore, are omitted in this model. Ion–atom and atom–atom interactions that are taken into consideration, the rate constants of the corresponding processes, and publications from which the rate constants were taken are listed in the table.

If the electric field in the discharge gap is sufficiently high (which is characteristic of a low-current discharge), the motion of atomic and molecular ions with taking into consideration their interactions (see the table) can be described by macroscopic transport equations and the motion of metastables can be described using corresponding diffusion equations [35–37]. After solving these equations by the finite difference method, we calculate number Δn_e of electrons generated in collisions between heavy particles per unit discharge volume per unit time (with regard to their recombination losses) and find the number of secondary electrons that should be added to cells of length Δz, into which the discharge gap is divided, to carry out Monte Carlo simulation of the electron kinetics.

Then, we again simulate the motion of electrons in the discharge gap with regard to additional secondary electrons and calculate the transport of ions and metastables. This procedure is repeated until the relative difference between the values of quantities in the succesive iterations becomes sufficiently small.

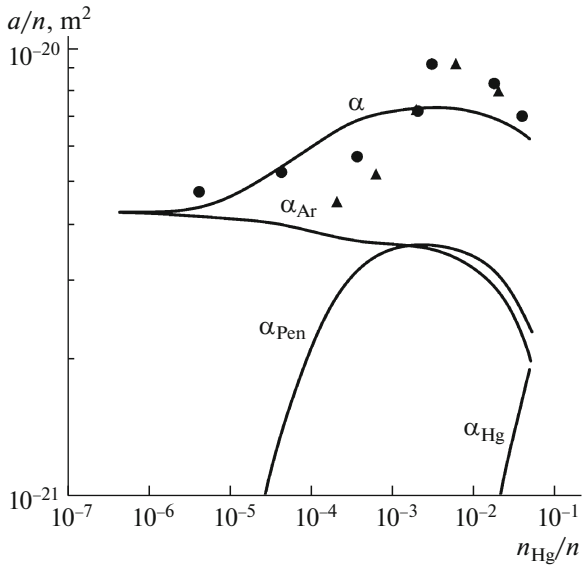

Fig. 3. Ionization coefficient and its components vs. the mercury relative concentration in the mixture for $E/n = 2.5 \times 10^{-19}$ V m^2. Lines describe calculation data, and symbols ● and ▲ are the experimental data of the ionization coefficient [12, 13].

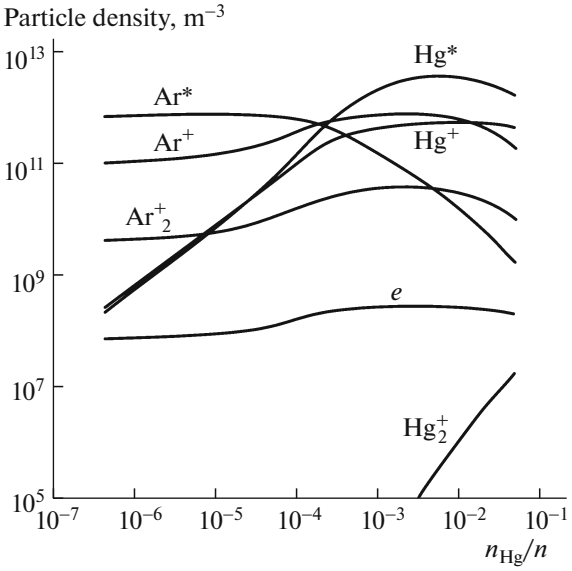

Fig. 4. Densities of the main types of charged and excited particles at the center of the discharge gap vs. mercury relative content n_{Ag}/n in the mixture for $E/n = 2.5 \times 10^{-19}$ V m^2.

After electron velocity distribution function $f_e(z_i, v, v_z)$ is found, one can calculate the ionization coefficient as a sum of terms that take into account contributions to it from the direct electron ionization of mercury and argon atoms and from ionization due to heavy particle collisions:

$$\alpha(z) = \alpha_{Ar}(z) + \alpha_{Hg}(z) + \alpha_{Pen}(z), \quad (1)$$

where

$$\alpha_{Ar}(z) = n_{Ar}\int\int \sigma_{iAr}(v) f_e(z, v, v_z) v dv dv_z / J_e(z),$$

$$\alpha_{Hg}(z) = n_{Hg}\int\int \sigma_{iHg}(v) f_e(z, v, v_z) v dv dv_z / J_e(z),$$

$$\alpha_{Pen}(z) = \Delta n_e / J_e(z),$$

$$J_e(z) = \int\int f_e(z, v, v_z) dv dv_z,$$

and $\sigma_{iAr}(v)$ and $\sigma_{iHg}(v)$ are the electron ionization cross sections of argon and mercury atoms, respectively.

The dependence of the ionization coefficient α and its components, as well as of other discharge characteristics, on coordinate z is due to the fact that the electron velocity distribution (at given electric field strength E) is almost equilibrium only at the center of the discharge gap, because of edge effects existing near the electrodes. At the center of the gap, the discharge characteristics reach their steady-state values [20, 38].

SIMULATION RESULTS AND DISCUSSION

Calculations were made for discharge gaps of length $d = 1.5 \times 10^{-3}$ m filled with pure argon, pure mercury vapor, and a mixture of argon (with Ar concentration $n_{Ar} = 6.57 \times 10^{23}$ m^{-3}, which corresponds to an Ar pressure of 2660 Pa at 20°C) and saturated mercury vapor. The density of the latter rapidly grows with temperature [39]. Therefore, the relative content n_{Hg}/n (where $n = n_{Ar} + n_{Hg}$) in the temperature interval from −30 to +130°C varies from 5×10^{-7} to 5×10^{-2} (Fig. 1). The discharge current density was taken to be equal to $j = 1 \times 10^{-5}$ A/m^2. For this value of the current density, the discharge is low-current at $U \sim 10^2$ V [5].

When the electron motion in the discharge was simulated, the number of secondary electrons emitted from the cathode was taken from the interval 10^3–10^4. It was assumed that their initial energies are uniformly distributed in the range 0–4 V and their escape directions are isotropically distributed within an angle with respect to the normal to the surface. The discharge gap, along with the ranges of variations in v and v_z, is split into 100 subintervals; that is, $s = 100$. When calculating the transport of ions and metastables in the mixture, because the mercury content is low, we used the mobilities of argon and mercury atomic and molecular ions in argon [27, 28, 40], as well as the diffusion coefficients of metastable ions of both gases in argon [28, 32].

Figure 2 plots the dependences of ionization coefficient α at the center of the discharge gap ($z = d/2$) on reduced electric field strength E/n in pure argon, pure mercury, and argon–mercury vapor mixture for $n_{Hg}/n =$

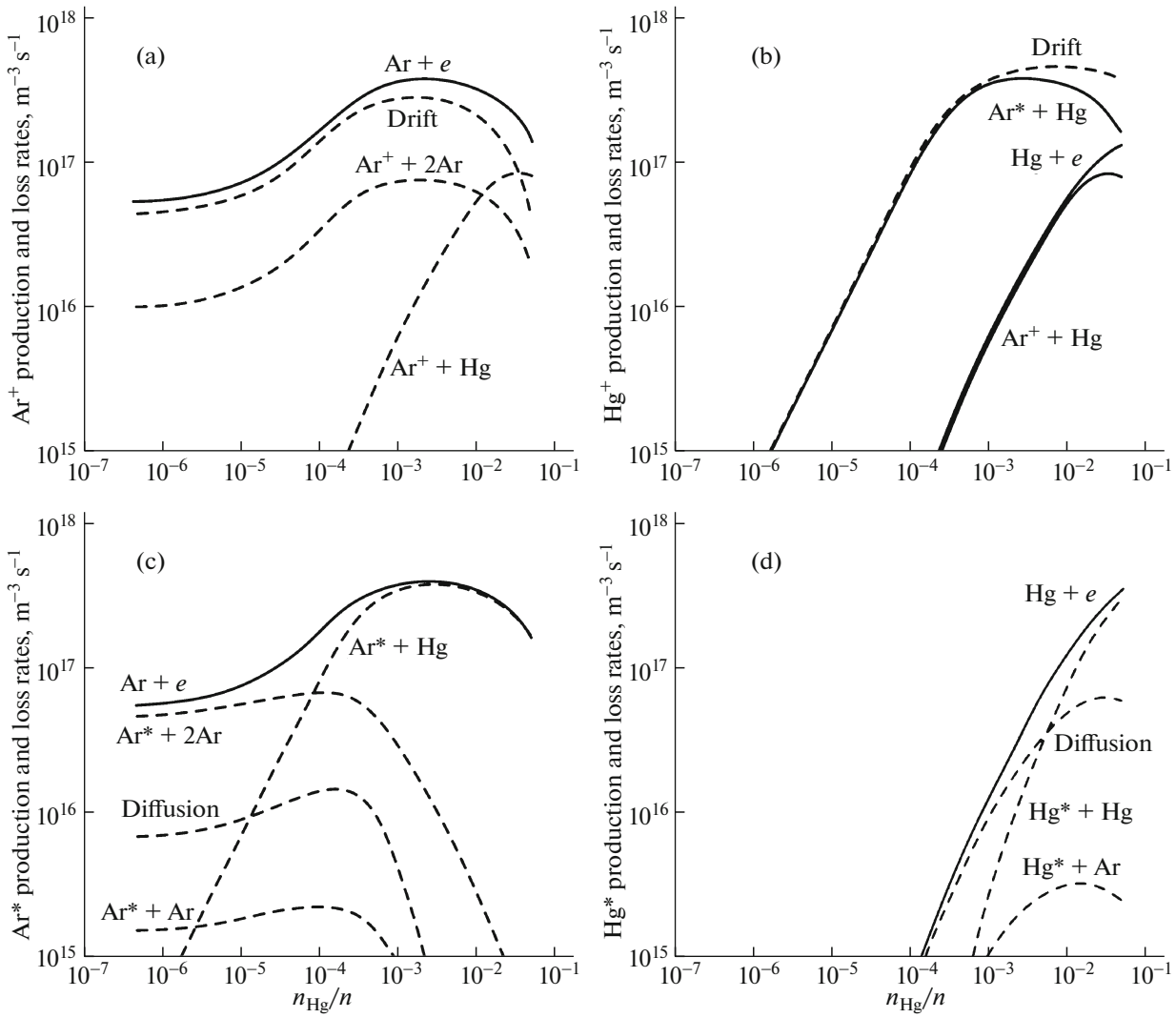

Fig. 5. Contributions of different mechanisms of production (solid lines) and loss (dashed lines) of atomic (a) argon and (b) mercury ions and (c) argon and (d) mercury metastables vs. the mercury relative content in the mixture for $E/n = 2.5 \times 10^{-19}$ V m^2.

6×10^{-3} along with the corresponding experimental data points [13, 41, 42]. It can be seen that the experimental data for α agree with calculations, which indicates the reasonable accuracy of the model used. The simulated dependence of the ionization coefficient in the argon–mercury mixture on the mercury relative content (Fig. 3) also agrees with the experiment. Note that the ionization coefficient reaches a maximum at $n_{Hg}/n \approx 5 \times 10^{-3}$. For argon density $n_{Ar} = 6.57 \times 10^{23}$ m^{-3} in the mixture, which is typical of high-pressure arc mercury lamps [4, 12], this takes place near 70°C; that is, the ionization rate at the stage of lamp ignition grows with ambient temperature. The term associated with the Penning ionization of mercury atoms by argon metastables makes a major contribution to quantity Δn_e, due to which the ionization coefficient in the argon–mercury mixture exceeds that in pure argon. The role of this term increases with decreasing electric field strength E. As for the direct ionization of mercury atoms by the electrons, its contribution is insignificant because the relative content of mercury atoms is low ($n_{Hg}/n < 10^{-2}$, Fig. 3).

The calculated dependences of the densities of ions and metastables at the center of the discharge gap on the mercury relative content in the mixture are shown in Fig. 4. It can be seen that, in the given interval of n_{Hg}/n, the main particles, along with electrons, are atomic ions and metastable excited atoms of mixture components, whereas the densities of molecular ions are at least by an order of magnitude lower (in agreement with the results of [19]). It follows from Fig. 5, which plots the discharge-gap-averaged contributions of the different mechanisms of particle generation and losses against n_{Hg}/n, that atomic argon ions Ar^+ arise as a result of the electron ionization of Ar atoms. As for

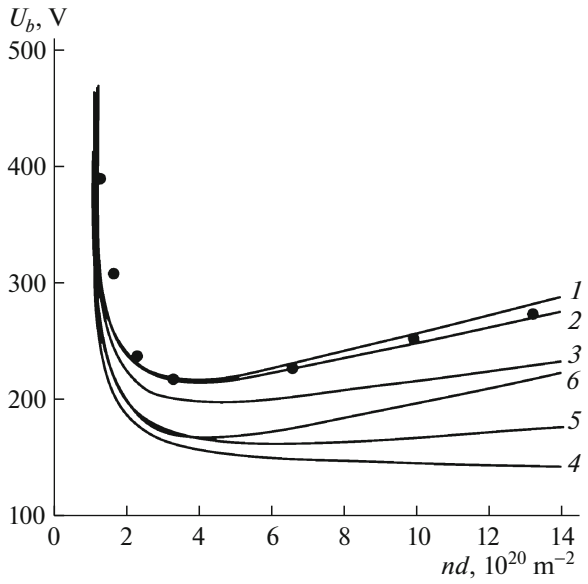

Fig. 6. Paschen curves in (*1*) argon and in the argon–mercury mixture at a temperature of (*2*) –10, (*3*) 10, (*4*) 70, (*5*) 90, and (*6*) 130°C. Symbols are experimental data points for U_b for the discharge in argon [43].

molecular mercury ions Hg^+, they arise mainly under the Penning ionization of mercury atoms by argon metastables at $n_{Hg}/n < 10^{-2}$, whereas at higher values of n_{Hg}/n direct ionization by electrons and nonresonance charge exchange between argon ions and mercury atoms also become significant. Ions of both types are lost because of their drift toward the cathode under the action of the electric field and, in addition, atomic argon ions may convert to molecular ions. Argon metastables Ar* appear as a result of the electron excitation of argon atoms and are lost (quenched) largely via collisions with unexcited argon atoms at $n_{Hg}/n < 10^{-4}$ and via the Penning ionization of mercury atoms when their density (n_{Hg}/n ratio) is higher. Mercury metastables Hg* arise from the electron excitation of mercury atoms. Then, they diffuse toward the electrodes and are deexcited in collisions with the surface at $n_{Hg}/n < 10^{-2}$ or, at higher values of $n_{Hg}/n > 10^{-2}$, are lost (quenched) in collisions with unexcited mercury atoms. Other particle–particle interaction mechanisms in the given interval of the discharge parameters may be disregarded.

It follows from Figs. 1–5 that, when the temperature of the mixture rises to 70°C and, hence, relative content n_{Hg}/n of mercury in the mixture rises to 5×10^{-3}, the rate of mercury ionization by argon metastables, electron density, and electron current density are increased. As a result, the ionization rate of mercury and argon atoms, the rate of argon atom electron excitation to metastable levels, and, consequently, the rate of Penning ionization of mercury atoms by argon metastables also grow. In this case, the densities of mercury ions and metastables and the ionization coefficient of the mixture are increased, whereas the density of argon metastables drops. When the temperature exceeds 70°C because of the rise in the mercury density, electron energy losses in collisions with mercury atoms grow considerably. As a result, the number of electrons with velocities sufficient for argon ionization decreases (in other words, the electron energy distribution narrows [19]). Accordingly, the rates of ionization of argon atoms by electrons and generation of argon metastables drop, which causes a reduction of the ionization coefficient of the mixture.

Using the calculated values of the ionization coefficient in the discharge gap, one can find the ignition voltage U_b of a discharge between the electrodes from the condition of discharge maintenance [5, 6]:

$$\int_0^d \alpha(z, U_b/d)dz = \ln(1 + 1/\gamma_{eff}), \qquad (2)$$

where γ_{eff} is the effective coefficient of ion–electron emission from the cathode.

The dependences of U_b on pd (p is the pressure of the gas mixture) or Paschen curves calculated from expression (2) for a discharge in an argon–mercury vapor mixture at different temperatures are shown in Fig. 6 (the value $\gamma_{eff} = 0.0125$ is taken from the condition that the value of U_b calculated in the minimum of the curve coincides with the corresponding experimental value for a discharge in pure argon, see [43]). This curve is in good agreement with the experimental one for the discharge in argon, whereas for the discharge in the argon–mercury mixture, U_b decreases when the temperature rises to 70°C and then grows with increasing temperature. This result follows from the nonmonotonic dependence of the ionization coefficient of the α mixture on n_{Hg}/n (Fig. 3) and is consistent with the experimental data in [10, 12].

CONCLUSIONS

In this work, we simulated the kinetics of the main types of charged and excited particles in an arc discharge initiated in an argon–mercury vapor mixture, which is used in gas-discharge illuminating lamps. The calculated dependences of the ionization coefficient on the reduced electric field strength in pure argon, pure mercury, and the argon–mercury vapor mixture, as well as the dependence of the ionization coefficient of the mixture on the mercury relative content in it, are in satisfactory agreement with the experimental data.

The temperature dependences of the contributions of different mechanisms behind the production and loss of ions and metastable atoms to maintaining their balance were determined. It was found that atomic argon ions are produced largely via the electron ionization of argon atoms and atomic mercury ions arise

mainly from the Penning ionization of mercury atoms by argon metastables. Both types of ions are lost mainly as a result of their drift toward the cathode under the action of the electric field. Metastables of argon and mercury appear when their atoms are excited by electrons, whereas argon metastables are lost due to the Penning ionization of mercury atoms and mercury metastables are quenched in collisions with excited atoms and during diffusion toward the electrodes. The influence of other processes on the densities of these ions is at least by an order of magnitude lower. The ionization coefficient in the argon–mercury mixture is higher than in pure argon almost exclusively because of the Penning reaction, the influence of which grows with decreasing electric field strength in the gap. We also calculated the dependences of the discharge ignition voltage on the size of the interelectrode gap (Paschen curves) for different temperatures of the mixture and explained the nonmonotonic dependence of the voltage on temperature. The obtained results may be helpful in estimating the influence of the gas mixture composition and the emissivity of the electrodes on the discharge ignition voltage in mercury illuminating lamps.

ACKNOWLEDGMENTS

This work was carried out in the framework of the Basic Research Program of the National Research University Higher School of Economics and also in the framework of the state task "Organization of Scientific Research" (Ministry of Education and Science of the Russian Federation) carried out at Bauman Moscow State Technical University.

REFERENCES

1. G. Zissis and S. Kitsinelis, J. Phys. D: Appl. Phys. **42**, 173001 (2009).
2. S. Samukawa, et al., J. Phys. D: Appl. Phys. **45**, 253001 (2012).
3. J. Schwieger, B. Baumann, M. Wolff, F. Manders, and J. Suijker, J. Phys.: Conf. Ser. **655**, 012045 (2015).
4. G. G. Lister, J. E. Lawler, W. P. Lapatovich, and V. A. Godyak, Rev. Mod. Phys. **76**, 541 (2004).
5. Yu. P. Raizer, *Gas Discharge Physics* (Dom Intellekt, Dolgoprudnyi, 2009; Springer, Berlin, 1991).
6. A. A. Kudryavtsev, A. S. Smirnov, and L. D. Tsendin, *Glow Discharge Physics* (Lan', St. Petersburg, 2010).
7. W. W. Byszewski, Y. M. Li, A. B. Budinger, and P. D. Gregor, Plasma Sources Sci. Technol. **5**, 720 (1996).
8. S. Hadrath, M. Beck, R. C. Garner, G. Lieder, and J. Ehlbeck, J. Phys. D: Appl. Phys. **40**, 163 (2007).
9. W. J. M. Brok, M. F. Gendre, and J. J. A. M. van der Mullen, J. Phys. D: Appl. Phys. **40**, 156 (2007).
10. A. Sobota, R. A. J. M. van den Bos, G. Kroesen, and F. Manders, J. Appl. Phys. **113**, 043308 (2013).
11. A. L. J. Burgmans and A. H. M. Smeets, J. Phys. D: Appl. Phys. **16**, 755 (1983).
12. A. E. Ataev, *Ignition of High-Pressure Mercury-Vapor Discharge Radiation Sources* (Mosk. Energ. Inst., Moscow, 1995).
13. S. Sawada, Y. Sakai, and H. Tagashira, J. Phys. D: Appl. Phys. **22**, 282 (1989).
14. V. M. Milenin and N. A. Timofeev, *Plasma of Low-Pressure Gas Discharge Sources of Light* (Leningrad. Gos. Univ., Leningrad, 1991).
15. G. Zissis, P. Bénétruy, and I. Bernat, Phys. Rev. A **45**, 1135 (1992).
16. N. Bashlov, G. Zissis, K. Charrada, M. Stambouli, V. Milenin, and N. Timofeev, J. Phys. D: Appl. Phys. **27**, 494 (1994).
17. G. M. Petrov and J. L. Giuliani, J. Appl. Phys. **94**, 62 (2003).
18. M. B. Ben Hamida, H. Helali, Z. Araoud, and K. Charrada, Phys. Plasmas **18**, 063506 (2011).
19. B. Lay, R. S. Moss, S. Rauf, and M. J. Kushner, Plasma Sources Sci. Technol. **12**, 8 (2003).
20. M. S. Mokrov and Yu. P. Raizer, Tech. Phys. **53**, 436 (2008).
21. E. A. Bogdanov, A. A. Kudryavtsev, and A. S. Chirtsov, Tech. Phys. **56**, 55 (2011).
22. E. Eylenceoğlu, I. Rafatov, and A. A. Kudryavtsev, Phys. Plasmas **22**, 013509 (2015).
23. S. D. Rockwood, Phys. Rev. A **8**, 2348 (1973).
24. A. V. Phelps, http://jilawww.colorado.edu/~avp/
25. H. A. Hyman, Phys. Rev. A **20**, 855 (1979).
26. A. Bogaerts and R. Gijbels, Phys. Rev. A **52**, 3743 (1995).
27. A. Bogaerts and R. Gijbels, J. Appl. Phys. **86**, 4124 (1999).
28. D. P. Lymberopoulos and D. J. Economou, J. Appl. Phys. **73**, 3668 (1993).
29. Y. Sakai, S. Sawada, and H. Tagashira, J. Phys. D: Appl. Phys. **22**, 276 (1989).
30. R. C. Wamsley, K. Mitsuhashi, and J. E. Lawler, Phys. Rev. E **47**, 3540 (1993).
31. M. A. Biondi, Phys. Rev. **90**, 730 (1953).
32. N. A. Kryukov, N. P. Penkin, and T. P. Red'ko, Opt. Spektrosk. **42** (1), 33 (1977).
33. L. A. Schlie, L. E. Jusinski, R. D. Rathge, D. L. Drummond, and R. A. Hamil, J. Appl. Phys. **51**, 3137 (1980).
34. S. E. Moody and R. E. Center, J. Appl. Phys. **55**, 2721 (1984).
35. V. I. Kristya and M. R. Fisher, Izv. Ross. Akad. Nauk, Ser. Fiz. **74**, 298 (2010).
36. V. I. Kristya and M. R. Fisher, Izv. Ross. Akad. Nauk, Ser. Fiz. **76**, 673 (2012).
37. G. G. Bondarenko, M. R. Fisher, and V. I. Kristya, J. Phys. Conf. Ser. **406**, 012031 (2012).
38. Z. Donkó, Plasma Sources Sci. Technol. **20**, 024001 (2011).
39. *Tables of Physical Quantities,* Ed. by I. K. Kikoin (Atomizdat, Moscow, 1976).
40. L. M. Chanin and M. A. Biondi, Phys. Rev. **107**, 1219 (1957).
41. H. N. Kucukarpaci and J. Lucas, J. Phys. D: Appl. Phys. **14**, 2001 (1981).
42. A. A. Garamoon and A. S. Abdelhaleem, J. Phys. D: Appl. Phys. **12**, 2181 (1979).
43. V. A. Lisovskiy, S. D. Yakovin, and V. D. Yegorenkov, J. Phys. D: Appl. Phys. **33**, 2722 (2000).

Translated by V. Isaakyan